Nonlinear Analysis of Epicardial Atrial Electrograms of Electrically Induced Atrial Fibrillation in Man

B.P.T. Hoekstra[1], C.G.H. Diks[1], M.A. Allessie[2] and J. DeGoede[1]

Journal of Cardiovascular Electrophysiology 1995, Vol. 6, No. 6, 419–440

[1]Department of Physiology, University of Leiden, The Netherlands
[2]Cardiovascular Research Institute Maastricht, Department of Physiology, Maastricht University, The Netherlands

Address for correspondence: B.P.T. Hoekstra, Leiden University Medical Center, Division of Image Processing, Department of Radiology, P.O. Box 9600, 2300 RC Leiden, The Netherlands. Tel: +31–71–526 2137; Fax: +31–71–526 6801; Email: B.P.T.Hoekstra@lumc.nl

Abstract

Introduction: We applied methods from the theory of nonlinear dynamics to characterize unipolar epicardial right atrial electrograms of electrically induced atrial fibrillation (AF) in man.

Methods and results: Electrograms were selected from a high-density mapping study (Konings et al., 1994) which confirmed the existence of at least 3 different types of induced AF (type I, II, III) in patients undergoing open-chest surgery. We analyzed sets of 5 electrograms (4 seconds, sampling frequency 1 kHz, resolution 8 bits) in 9 patients (AF type I, n=3, type II, n=3, type III, n=3). The Grassberger-Procaccia method was applied to estimate the correlation dimension and correlation entropy from the electrograms. In 2 patients (AF type I) some electrograms (2 and 3 out of 5, respectively) showed scaling at normalized distances ranging from 0.2 to 0.5 in phase space. Correlation dimension D ranged from 1.8 to 3.2 and correlation entropy K from 2.2 to 3.8 nats/s. The patients were ranked according to increasing coarse-grained correlation dimension D_{cg} (range 3.7 to 7.9) and coarse-grained correlation entropy K_{cg} (range 5.6 to 18.6 nats/s). The method of surrogate data was applied to detect nonlinearity in the electrograms. Using the correlation integral as test statistic, it could be excluded that electrograms of type I of AF have been generated by linear stochastic dynamics. Episodes of sinus rhythm (D ranging from 1.0 to 5.1 and K from 2.0 to 8.6 nats/s) and induced atrial flutter (D ranging from 2.7 to 4.2 and K from 2.2 to 4.2 nats/s) in 2 different patients showed features of low-dimensional chaos.

Conclusion: Nonlinear analysis discriminated between electrograms during electrically induced AF in humans. The results are consistent with a classification of AF into 3 types based on the spatio-temporal complexity of right atrial activation patterns.

nonlinear dynamics, time series analysis, atrial fibrillation, high-density mapping

Introduction

Clinically, atrial fibrillation is usually regarded as a single entity based on simple ECG criteria such as absence of P waves and total irregularity of QRS complexes.

The development of advanced high-density mapping techniques has provided the opportunity to monitor in great detail the cardiac electrical excitation and it has been demonstrated that atrial fibrillation is based on multiple reentering wavelets.[1] Based on the morphological characteristics of a single bipolar atrial electrogram, in 1978 Wells et al.[2] distinguished different types of atrial fibrillation. A mapping study of electrically induced atrial fibrillation in humans has recently confirmed the existence of at least three types of atrial fibrillation.[3]

Clinically, it might be of importance to be able to characterize atrial fibrillation from single local electrograms and to discriminate between different types of fibrillation.

In the last two decades a large number of methods from nonlinear dynamical systems theory have been developed to analyze experimental time series. Using a theorem proven by Takens[4,5] one can reconstruct the phase space of a deterministic system from a measured time series and extract properties of the underlying dynamics. These methods have been applied to characterize cardiac time series both during normal[6–8] and pathological conditions. They have been useful, for example, to detect changes in the dynamics of RR intervals in high-risk patients of sudden cardiac death shortly before the onset of ventricular fibrillation.[9]

The purpose of the present study was to apply mathematical methods from the theory of nonlinear dynamics to characterize and classify unipolar epicardial electrograms of electrically induced atrial fibrillation in humans. The results of the nonlinear analysis are compared with a recently proposed classification of atrial fibrillation into three types based on the degree of spatio-temporal complexity of human atrial activation patterns.[3]

Methods

Data were derived from the high-density mapping study of Konings et al.[3] in which atrial fibrillation was induced in 25 patients undergoing open-chest surgery for interruption of accessory conduction pathways (Wolff-Parkinson-White syndrome).

Data acquisition

Local epicardial electrical activity was recorded by an octagonal electrode matrix (diameter 3.6 cm, interelectrode distance 2.25 mm) containing 244 unipolar electrodes (silver wires, diameter 0.3 mm). Figure 1 shows the mapping electrode positioned at the free wall of the right atrium.

Multiple recorded electrograms were amplified (gain 150 to 1000), filtered (bandwidth 1 to 500 Hz), multiplexed (sampling rate 1 kHz) and AD converted (resolution 8 bits). Details of the mapping system have been described elsewhere.[10]

High-density mapping of atrial fibrillation

Since the results of the nonlinear analysis will be compared to the results of the high-density mapping study of Konings et al.,[3] we will here briefly summarize some of their findings. Maps of electrically induced atrial fibrillation were classified into three categories (I, II and III) based on the degree of complexity of activation of the free wall of the right atrium. Type I fibrillation was characterized by single waves, changing their main direction in the course of time, but propagating uniformly and showing no major intra-atrial conduction delays or block. During type II fibrillation two wavelets were present most of the time,

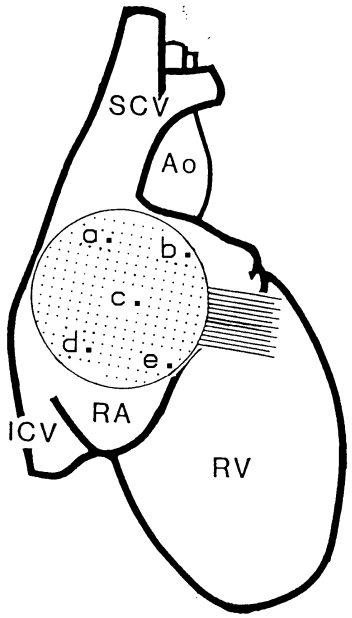

Figure 1: Mapping of the free wall of the human right atrium using a 244-lead epicardial mapping electrode (interelectrode distance 2.25 mm). Positions (a) to (e) indicate the electrode leads chosen for analysis. Ao aorta; ICV inferior caval vein; SCV superior caval vein; RA right atrium; RV right ventricle. Modified from Konings et al.,[3] with permission.

entering the mapping area from different directions. Both local areas of slow conduction as well as lines of functional conduction block were present separating the two wavefronts. Type III maps were highly complex with multiple wavelets entering and leaving the mapping area at different sites. Delayed conduction and turning of wavelets around multiple arcs of intra-atrial conduction block were frequently observed.

An incidence of more than 50 % of type I or type III maps was chosen as the boundary between the three types (I, II, III) of atrial fibrillation. Going from relatively simple to highly complex atrial activation, both the atrial rate of fibrillation and the variation in fibrillation intervals gradually increased. In Figure 2, examples of right atrial activation patterns of type I, II and III atrial fibrillation are shown.

Data selection

From the 25 patients studied by Konings et al.[3] 9 patients were selected for our analysis. Three patients were classified as type I, three as type II and three as type III fibrillation. Patient characteristics are summarized in Table 1.

From each patient a segment of 4 seconds of atrial fibrillation was analyzed. In addition from patient 1 an episode of sinus rhythm (16 seconds, down sampled by a factor 4) and from patient 8 an episode of electrically induced atrial flutter (6 seconds) were analyzed

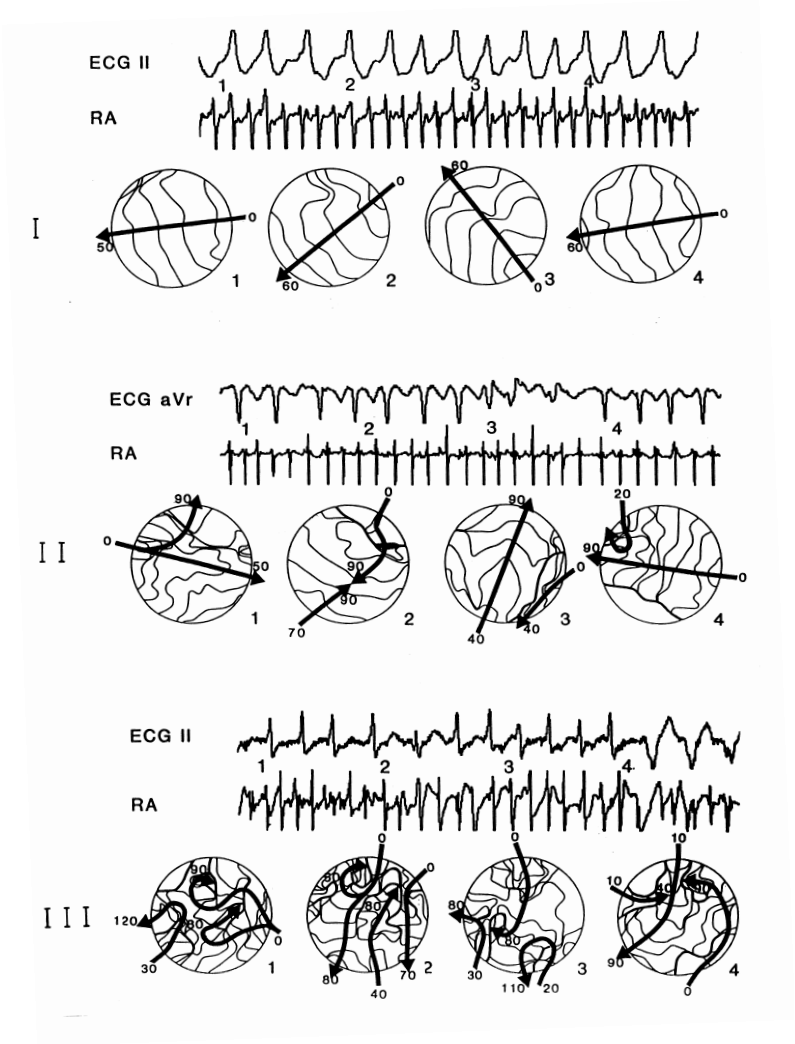

Figure 2: Surface ECG, a right atrial unipolar electrogram (RA), and activation maps of the right atrial free wall during electrically induced atrial fibrillation. From the study of Konings et al.[3] Top, Type I atrial fibrillation (patient 11). Activation maps were taken at 1-second intervals. Isochrones have been drawn at 10-millisecond intervals. Arrows indicate the main directions of activation. In this case, the right atrium was activated by a single depolarization front changing its main course of direction with time. No areas of slow conduction were found, and the total conduction time under the mapping electrode varied from 50 to 60 milliseconds. Middle, Type II atrial fibrillation (patient 7). Most of the time, two wavelets were present under the mapping electrode. In map 1 the entering wavelet (t=0) branched into two separate fronts. In map 2 two different wavelets entered the mapping area at t=0 and t=70 respectively, and subsequently collided at t=90 milliseconds. Areas of slow conduction (crowding of isochrones) as well as local arcs of conduction block (thick lines) were present and the conduction time needed to cross the mapping area was prolonged to 90 milliseconds. Bottom, Type III atrial fibrillation (patient 3). Activation patterns were highly fragmented and the mapping area was continuously occupied by multiple wavelets, entering and leaving the mapping area at different sites and at different times. Often, the wavelets reentered areas which had been previously excited by another wavelet (random reentry). ECG traces (leads II and aVr) show irregular incidence of QRS complexes and a varying degree of preexcitation.

Table 1
Patient characteristics

Patient no.		Age, y	Sex	Type of map, % *			Type of AF	Interval, ms **	
				I	II	III		Median	P_{5-95}
1	21	52	F	100	0	0	I	193	42
2	11	36	F	90	10	0	I	150	59
3	15	27	M	79	21	0	I	140	87
4	5	28	F	27	69	4	II	140	115
5	7	45	M	20	68	12	II	138	73
6	20	31	F	0	56	44	II	141	93
7	18	34	M	3	28	69	III	118	65
8	3	23	M	6	10	84	III	143	116
9	16	37	M	0	4	96	III	121	87
		35±9 †							

*Relative incidence in time windows of 12 seconds. In patient 9, only 4 seconds were analyzed because of short duration of AF. **Results of fibrillation interval histograms using five electrograms of the mapping area. P_{5-95} denotes the difference between the 5th and 95th histogram percentiles. The second column refers to patient numbers in Konings et al.[3] AF atrial fibrillation; F female; M male. †Mean ± SD.

for comparison. The length of the analyzed electrograms corresponded to about 20 to 30 activation intervals.

From the available 244 electrograms, five were chosen at positions (a) through (e) as indicated in Figure 1. The distance from the four outer electrodes to the centre electrode (c) was 16.2 mm. We checked by visual inspection whether the electrograms showed obvious transients or artifacts and whether the signal to noise ratio was satisfactory. In case a signal was not considered suitable for analysis, a neighbouring electrogram was chosen.

Reconstructing dynamics from time series

The application of the theory of nonlinear dynamics, more commonly known as "chaos theory", is relatively new in the field of cardiology. Therefore, in Table 2 we give a list of definitions which may serve as a glossary of the terms used. For a more extensive introduction to chaos theory we refer the interested reader to Ott et al.[11]

Before describing the mathematical methods used in more detail, we illustrate the essential steps of the nonlinear analysis in Figure 3. We start with a time series (upper panel) and plot the values against delayed values in a so-called phase plot (step 1). This gives a first impression of the underlying dynamics, note the geometrical structure displayed in the phase plot. Next, the correlation integral $C_m(r)$ is calculated for different embedding dimensions m (step 2). Two cases should be distinguished. If the correlation integral shows

Table 2
Glossary

Attractor: Bounded and connected part in phase space towards which the state of the system is attracted in the course of time. An attractor is thus a geometrical object in phase space.
Chaos: Aperiodic, seemingly random behaviour in a deterministic nonlinear system. Chaos can only occur in nonlinear dynamical systems.
Chaotic dynamics: We speak of chaotic dynamics when the trajectory in phase space "lives" on a strange attractor.
Correlation integral: Mathematical quantity from which the correlation dimension and correlation entropy are calculated.
Correlation dimension: Measure of the "geometrical complexity" of an attractor.
Correlation entropy: Measure of the "dynamical complexity" of an attractor.
Coarse-grained correlation dimension/entropy: The correlation dimension/entropy at a finite (coarse-grained) resolution in state space.
Delay vector: Represents a point in reconstructed phase space.
Deterministic system: System which can be described without using concepts from probability theory.
Dynamical system: Mathematical model of a real world system.
Embedding dimension: Number of points in a segment of the time series used to reconstruct phase space.
Embedding delay: Time delay between successive points in a segment of the time series used to reconstruct phase space.
Grassberger-Procaccia (GP) method: Mathematical method to estimate the correlation integral, correlation dimension and entropy from a measured time series.
High-dimensional chaos: Chaos for which the correlation dimension is high (say > 5).
Low-dimensional chaos: Chaos for which the correlation dimension is low (say < 5).
Method of surrogate data: Method to test the presence of nonlinearity in a time series.
Mutual information function: Measure of the (nonlinear) correlation between two time series shifted in time with respect to each other.
Nonlinearity: Property of a system for which the output is not linearly proportional to the input.
Nonlinear dynamical system: Dynamical system for which the sequence of states in time is related nonlinearly.
Phase plot: Two-dimensional graph of the values in the time series plotted against time delayed values.
Reconstructing dynamics: Mathematical procedure to reconstruct phase space with delay vectors.
Reconstruction parameters: Quantities to be chosen in the reconstruction of the dynamics, e.g. the embedding delay and the embedding dimension.
Scaling region: A linear region in a double logarithmic plot of the correlation integral versus distance in phase space.
State space (phase space): The time dependence of the state variables can be visualized as a trajectory in an m-dimensional state or phase space (m is the number of state variables).
Strange (chaotic) attractor: When two points on an attractor which are originally close together depart from each other so that their distance increases exponentially in time, the attractor is called strange (or chaotic).
Surrogate time series: Artificially generated data, in which the linear properties of the original time series are preserved.
Trajectory: The time course of the state of the system in phase space.

scaling (a linear part on a double logarithmic scale, indicated between dashed lines, lower left panel), the correlation dimension D and correlation entropy K are estimated (step 3). If the correlation integral shows no scaling (no linear part, lower right panel), a distance r (asterisk) and an embedding dimension m (thick line) are chosen at which the coarse-grained correlation dimension D_{cg} and the coarse-grained correlation entropy K_{cg} are estimated (step 3). The coarse-grained quantities are also assessed when there is scaling. The time series, phase plot and correlation integrals in the lower left panel originate from the x-component of the Rössler system.[12] The correlation integrals in the lower right panel are calculated for a time series generated by Gaussian white noise.

The mathematical description of the dynamical behaviour in a variety of physical, biological and other systems contains two elements: the state of the system and an evolution law. The state of a given system at time t is completely specified by a set of continuous parameters, called the state variables. The dynamics of the state variables are governed by an evolution law which tells the system how to get from the state at time t to the state at a later instant. If the evolution law relates the states in a unique way, the mathematical description is called a (deterministic) dynamical system. If, however, the sequence of states in time is determined by chance we speak of a stochastic (dynamical) system. Furthermore, if different states of a dynamical system are related by a linear law the dynamics are linear; otherwise the dynamics are called nonlinear.

During an experiment one does not have access to all state variables, and only a limited number of variables can be measured as a function of time, often just one. The measurement of that variable is stored in a time series $\{h(t_i)\}_{i=1}^{N}$, consisting of N measurements at discrete times t_i. The laws which generate the experimental data are unknown, but we would like to reconstruct the underlying dynamics of the observed variable. In the simplest case the state of the system would be fully determined by just one variable. In general, however, the state of the system will consist of many state variables. The key idea in nonlinear analysis to faithfully reconstruct the dynamics is to take as state variables the measured points in a segment of the observed time series, say m points. To this end one starts with taking a sample $h(t_i)$ of the time series. Next, samples each separated by a so-called embedding delay τ are taken until m samples have been collected. These values of the time series are used as the components of a delay vector defined as

$$\vec{x}(t_i) = (h(t_i - (m-1)\tau), \ldots, h(t_i - 2\tau), h(t_i - \tau), h(t_i)), \tag{1}$$

which represents the state of the system at time t_i. The next reconstructed state is found in a similar way by advancing the time index i by the sampling period and repeating the procedure. In this way a cloud of delay vectors (points) is reconstructed in a so-called state or phase space with embedding dimension m.

The mathematical justification of this reconstruction technique constitutes the content of Takens' reconstruction theorem[4] and is basic to nonlinear time series analysis. This

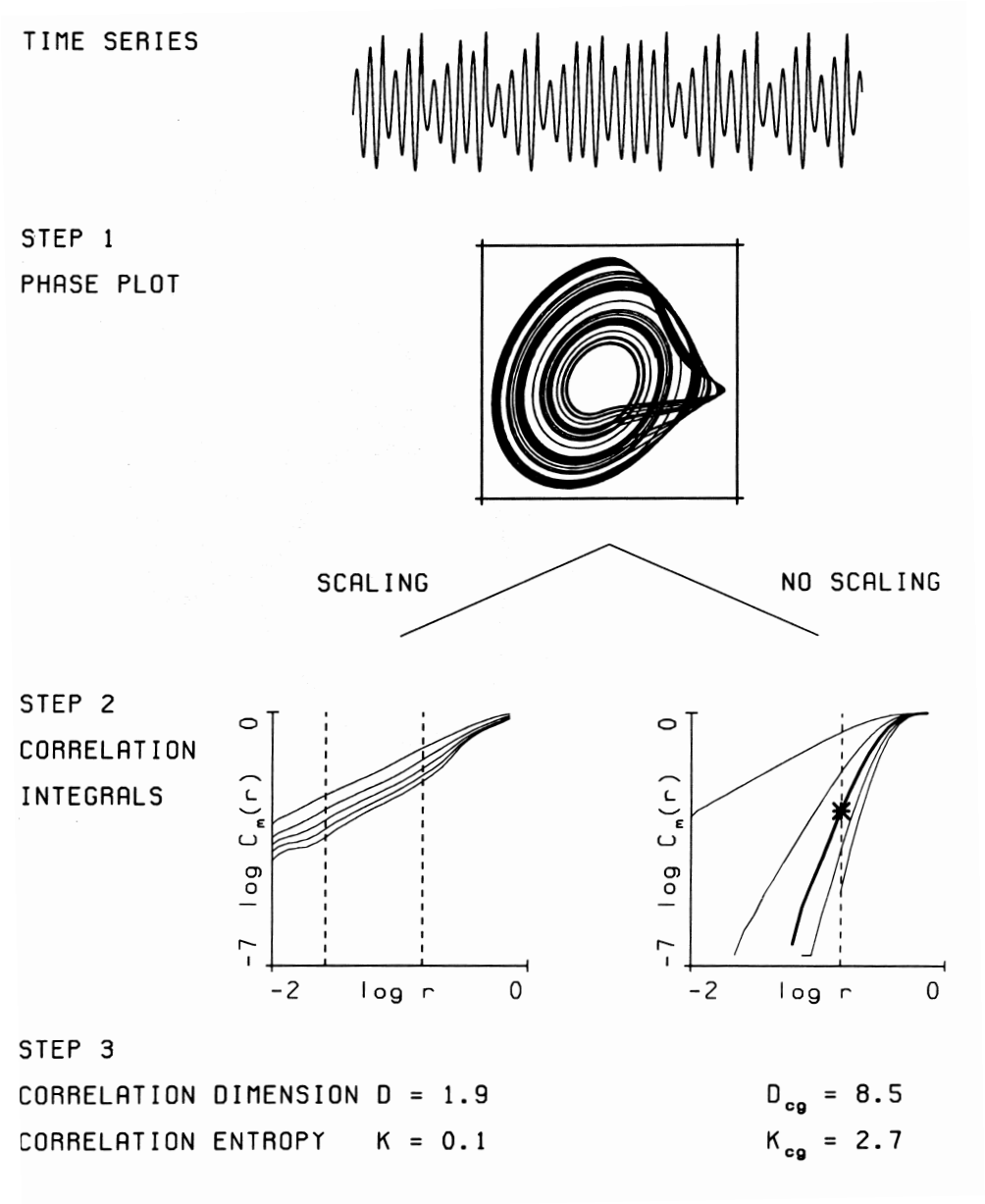

Figure 3: Schematic diagram illustrating the essential steps in the nonlinear analysis. See text for explanation. The time series, phase plot and correlation integral $C_m(r)$ (lower left panel) originate from a time series (4000 samples) generated by the x-component of the Rössler system.[12] The correlation integral is plotted at embedding dimension $m = 2$, 6, 10, 14, 18 (top to bottom curves). A scaling region is indicated between dashed lines. Estimated correlation dimension $D = 1.9$ and correlation entropy $K = 0.1$ nats/s. The correlation integrals in the lower right panel are calculated for a time series (4000 samples) generated by Gaussian white noise. The coarse-grained correlation dimension $D_{cg} = 8.5$ and coarse-grained correlation entropy $K_{cg} = 2.7$ nats/s are evaluated at normalized distance $r = 0.15$ (asterisk) and embedding dimension $m = 10$ (thick line).

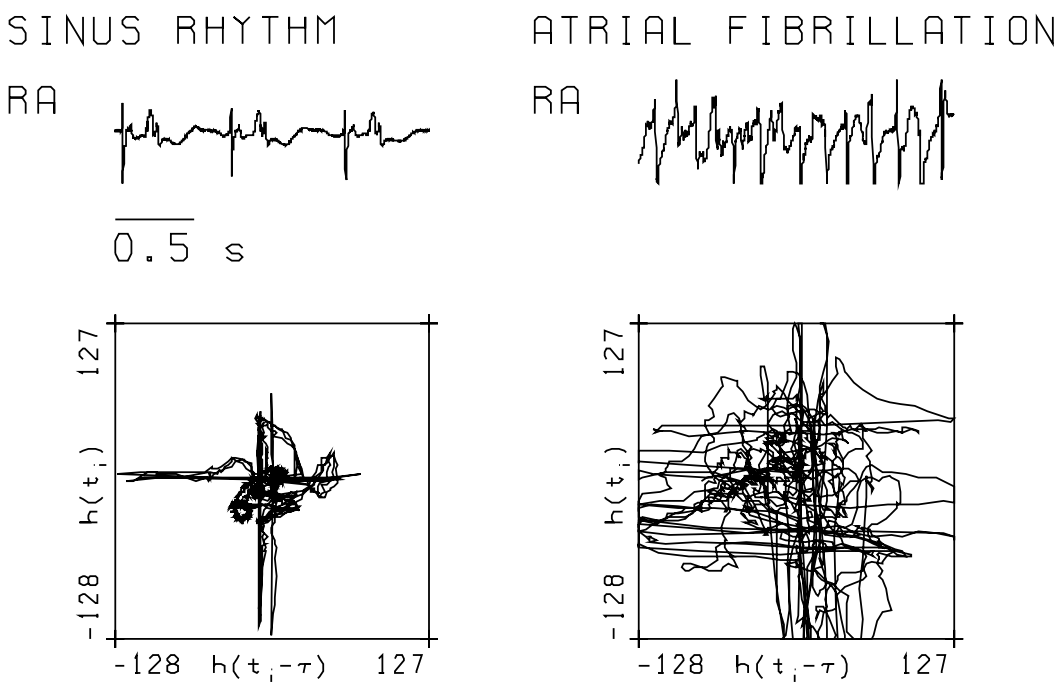

Figure 4: A unipolar epicardial right atrial electrogram (RA) of sinus rhythm (patient 1) and atrial fibrillation (patient 8). Bottom, the corresponding phase plots for the range of discrete times t_i. The embedding delay τ was 35 ms for the episode of sinus rhythm and 40 ms for atrial fibrillation. Trajectories of sinus rhythm show a cross-like structure. Additional fine structure is visible resulting from e.g. ventricular deflections. Trajectories of atrial fibrillation show a more complex structure resulting from both discrete activation complexes and irregular deflections. The recorded extracellular voltages were about 1 to 10 mV. Typical gains used were 300 to 1000. The resolution after AD conversion was 8 bits.

theorem guarantees that the dynamical characteristics of the real (physiological) and the reconstructed system are the same.

A first impression of the underlying dynamics of the observed time series, viz. the evolution law, can be obtained by drawing a two-dimensional phase plot. To this end, the values of the time series at time t_i and at $t_i - \tau$ are plotted against each other. Repeating this procedure for consecutive time indices i, the points in the phase plot trace out a trajectory, which visualizes the time course of the two-dimensional delay vector $(h(t_i - \tau), h(t_i))$. The embedding delay time τ is a properly chosen multiple of the sampling period.

In Figure 4, unipolar epicardial right atrial electrograms are shown during sinus rhythm and atrial fibrillation. Phase plots are drawn using a delay τ of 35 ms and 40 ms, respectively. Activation during sinus rhythm resulted in cross-like trajectories. Additional fine structure is visible resulting from e.g. ventricular deflections. The phase plot of atrial fibrillation shows a more complex structure resulting from both discrete activation and irregular deflections.

Estimating correlation dimension and entropy

In general the time dependence of the set of state variables can be thought of as a trajectory in an abstract mathematical space called state space or phase space. When the evolution law of the system attracts the states to a bounded subset of phase space in the course of time, this subset is called an attractor. We speak of chaotic dynamics when the behaviour of a deterministic dynamical system on an attractor is aperiodic and seemingly random. In that case the attractor is called strange or chaotic.

The correlation integral has been introduced[13,14] to characterize chaotic dynamics. Grassberger and Procaccia proposed a by now standard method (GP) to estimate the correlation integral from a measured time series. The GP method starts with reconstructing m-dimensional phase space from a time series using delay vectors (eq. 1). Next, a reference point (delay vector) is chosen in phase space. This point is reconstructed using m samples of the time series, each separated by an embedding delay τ. The reference point thus contains information which originates from a segment in the time series. A neighbouring point in phase space corresponds in turn to a different segment in the time series. The correlation integral counts the number of neighbouring points in phase space around the chosen reference point. Therefore the correlation integral accounts for the number of different time segments which "look like" the chosen reference segment. How closely a given time segment resembles the reference segment, is mathematically expressed by a "distance" r between the two points in phase space. The larger the distance is, the more the time segment differs from the reference segment.

The counting of neighbouring points is repeated for a large number of randomly chosen reference points in phase space. The results at each distance r are averaged and normalized to the total number of counted points. The resulting value constitutes the correlation integral $C_m(r)$ at distance r in reconstructed phase space of embedding dimension m. The GP method is commonly used to calculate two parameters of the underlying dynamics from the correlation integral, viz. the correlation dimension and correlation entropy.

In terms of the GP method the correlation dimension D estimates the average density of points in phase space around reference points, when we look at smaller and smaller differences between the time segments. This amounts mathematically to letting the distances between points in phase space go to zero. The correlation dimension is thus associated with the organisation of points in phase space and is a measure of the geometrical complexity of the supposed attractor. In general, a strange attractor is characterized by a finite non-integer correlation dimension. A more complex dynamics will result in a larger value of the correlation dimension. If the dynamics are stochastic, D is equal to infinity. An alternative interpretation worth mentioning here is that, roughly speaking, the correlation dimension gives the number of state variables needed to describe the dynamics "living" on the attractor with a deterministic model.

The correlation entropy K is a measure of how fast the distance between two initially

nearby states in phase space grows in time. This can be envisaged by taking a point in reconstructed phase space, which corresponds to a segment in the time series. Another point in phase space located closely to the first point refers to a different segment in the time series. Correlation entropy is a measure of how fast these time segments loose their resemblance when both the segments are lengthened, looking at finer and finer details. Correlation entropy is therefore a measure of the "wildness" of the dynamics. One may also interpret correlation entropy as the rate at which information is lost about the state of the system in the course of time. In general a larger value of the correlation entropy corresponds to a more complex dynamics. K is positive (but finite) for chaotic dynamics, and infinite for stochastic dynamics.

The procedure to estimate D and K from the correlation integral is to draw a double logarithmic plot of the correlation integral as a function of distance r in reconstructed phase space. At a given embedding dimension m one then looks for a linear part, a so-called "scaling region", in this double logarithmic plot.

The correlation dimension D at embedding dimension m can be estimated as the slope of the correlation integral in the scaling region. In case D saturates as a function of m, this value is taken as the correlation dimension. The correlation entropy K can be estimated from the double logarithmic plot by the rate of lowering of the correlation integrals within the scaling region with increasing embedding dimension m. The procedure follows from the structure of the Grassberger-Procaccia correlation integral. We refer to the appendix for a description of the implementation to estimate the correlation integral, the correlation dimension and entropy from a measured time series.

We give an example to illustrate the calculation methods, using a 16 second right atrial electrogram of sinus rhythm down sampled to 4000 points. An embedding delay τ of 52 ms was used to construct delay vectors in a phase space up to embedding dimension 20. In Figure 5 (left column), calculated correlation integrals $C_m(r)$ are drawn in a double logarithmic plot as a function of distance r (upper left panel). Embedding dimension m ranges from 2 (top curve) to 20 (bottom curve) incremented by 2. A scaling region (between dashed lines) was chosen in the interval [0.04-0.18] of normalized distance r.

The middle panel shows the local slope of the correlation integrals as a function of distance r for the range of embedding dimensions m. Starting at the lowest values resulting from the slope of the correlation integral at embedding dimension 2 (bottom curve), the slope within the scaling region saturated with increasing embedding dimension m, as is observed from the "plateauing" of the top curves. Averaging the slopes in the scaling region over embedding dimensions 15 to 19 resulted in a correlation dimension $D = 3.8 \pm 0.1$ (mean $\pm$ SD).

As can be seen in the upper left panel the rate of lowering of the correlation integrals is largest when the embedding dimension m is relatively small (top curves). The distance between successive correlation integrals within the scaling region gets smaller when embedding dimension is increased and gets more or less constant (bottom curves). This is reflected

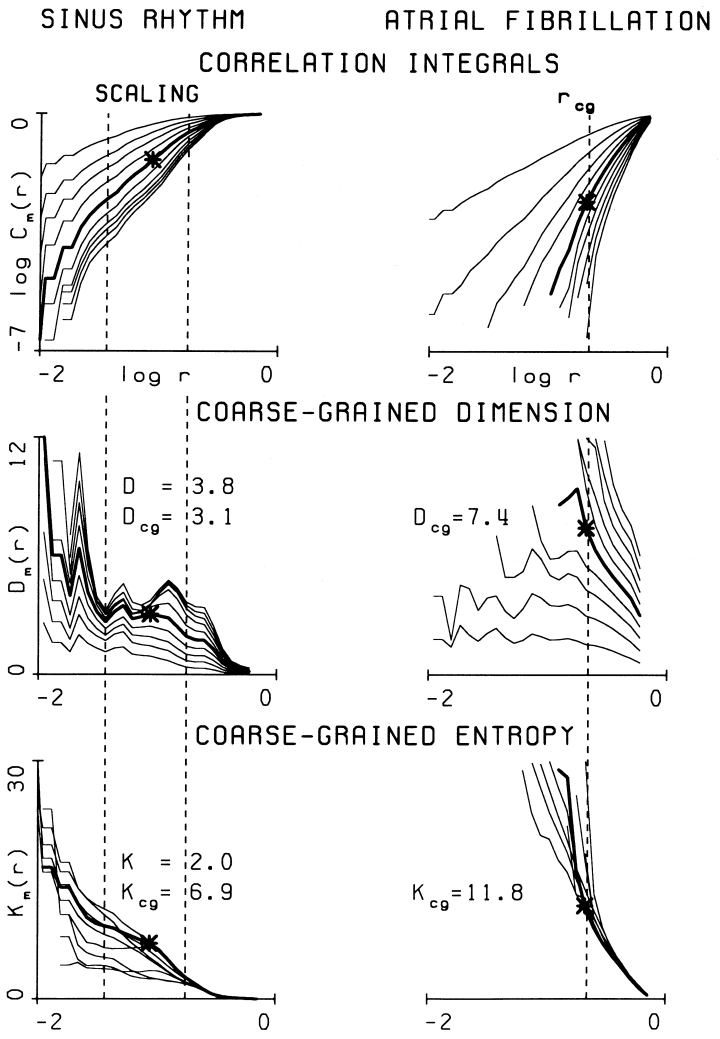

Figure 5: Correlation integrals $C_m(r)$, coarse-grained dimension $D_m(r)$ and coarse-grained entropy $K_m(r)$ of sinus rhythm (left column, patient 1) and electrically induced atrial fibrillation (right column, patient 8). Double logarithmic plots $\log_{10} C_m(r)$ versus normalized distance $\log_{10}(r)$ show correlation integrals for embedding dimensions $m = 2$ (top curve) to 20 (bottom curve), with an increment of 2. Coarse-grained dimension D_{cg} and coarse-grained entropy K_{cg} were estimated at embedding dimension 10 (thick lines) and at a coarse-grained resolution r_{cg} (asterisk), corresponding to the normalized standard deviation of the electrogram. Results are shown for an electrogram of 16 seconds of sinus rhythm (patient 1) and 4 seconds of atrial fibrillation (patient 8). During sinus rhythm the coarse-grained dimension D_{cg} was 3.1 and the coarse-grained entropy K_{cg} was 6.9 nats/s at a resolution r_{cg} of 0.09. The episode of atrial fibrillation was characterized by a coarse-grained dimension D_{cg} of 7.4 and a coarse-grained entropy K_{cg} of 11.8 nats/s at a resolution r_{cg} of 0.22. During sinus rhythm a scaling region was selected in interval [0.04-0.18] of normalized distances (between dashed lines) where correlation integrals show a linear part in the log-log plot. Averaging the results within the scaling region over embedding dimensions 15 to 19 resulted in a correlation dimension $D = 3.8 \pm 0.1$ and correlation entropy $K = 2.0 \pm 0.1$ nats/s.

in the lower left panel, where larger values correspond to a larger entropy. It is observed that the entropy values saturate within the scaling region as embedding dimension m is increased (from top to bottom curves). The estimated correlation entropy was averaged over embedding dimensions 15 to 19 and converged to $K = 2.0 \pm 0.1$ nats/s.

If the reconstructed dynamics from an observed time series can not be described by the Grassberger-Procaccia correlation integral, e.g. because there is no convincing scaling region, the correlation integral can nevertheless be used to extract so-called coarse-grained dimensions and entropies.[15–17] These coarse-grained measures characterize the correlation integral at a finite resolution in phase space and still quantify the complexity of the dynamics.

Coarse-grained correlation dimension is a rough measure of the complexity of the attractor and can be envisaged as follows. When the resolution in phase space is coarse, the location of a neighbouring point with respect to a reference point can be determined up to a precision which is limited by a coarse-grained resolution (distance in phase space) r_{cg} between the two points. Coarse-grained correlation dimension $D_m(r)$ is defined by the local slope of the correlation integral at distance r_{cg} in phase space of embedding dimension m.

Coarse-grained correlation entropy is a measure for the distance between two points in phase space to increase beyond the coarse-grained resolution r_{cg} when embedding dimension m is increased. It is a measure of how fast two segments in the time series which initially resemble each other start to look different when the size of the segments is enlarged. Coarse-grained correlation entropy $K_m(r)$ is estimated from the amount of lowering of the correlation integral at distance r_{cg} in phase space when embedding dimension m is increased. We refer to the appendix for a description of the implementation to estimate the coarse-grained correlation dimension and entropy.

In the right column of Figure 5 we give an example of the calculation of these coarse-grained quantities, using a 4 second right atrial electrogram of electrically induced atrial fibrillation. An embedding delay τ of 46 ms was used to construct delay vectors in phase space up to embedding dimension 20. We calculated correlation integrals (upper right panel) and evaluated the coarse-grained correlation dimension D_{cg} (middle right panel) and coarse-grained correlation entropy K_{cg} (lower right panel) at embedding dimension m =10 (thick lines). The coarse-grained resolution r_{cg} (asterisk) was chosen equal to a normalized standard deviation, which was calculated dividing the standard deviation of the electrogram by the largest absolute difference of the amplitudes of the signal. In this example coarse-grained dimension D_{cg} was 7.4 and the coarse-grained entropy K_{cg} was 11.8 nats/s at $r_{cg} = 0.22$. During sinus rhythm (left column) the estimated values for D_{cg} and K_{cg} were 3.1 and 6.9 nats/s, respectively at $r_{cg} = 0.09$.

Detecting nonlinearity

The method of surrogate data was developed by Theiler et al.[18,19] to identify nonlinearity in time series. Since nonlinearity is a necessary condition for chaotic dynamics, this technique

is widely applied to indicate the possibility of the existence of chaos in an observed time series.

The method compares the original time series with artificially generated random series, so-called "surrogate data", which are constructed to mimic the linear properties of the original series. The properties of the surrogate data are used to test the null hypothesis that the observed time series is generated by linear stochastic dynamics. The original and the surrogate series are compared using a proper statistic. When the difference between the original series and a set of surrogate time series is statistically significant, the null hypothesis can be rejected. This means that there is evidence for nonlinearity being present in the dynamics which generated the original time series. However, this does not mean that the underlying dynamics is necessarily chaotic. The method of surrogate data can be used to exclude certain classes of stochastic dynamics, but a definite positive indication of chaos in the observed time series can not be inferred.

We have applied an algorithm[19] to create surrogate data having the same sample mean, variance, spectral density and amplitude distribution as the original electrogram. Using the GP method, correlation integrals were calculated for an ensemble of 10 surrogate time series. We used the correlation integral as a statistic to discriminate between the mean correlation integral of the ensemble of surrogate data and the correlation integral of the electrogram at embedding dimension 10. If the difference is statistically significant, the null hypothesis can be rejected.

Figure 6 shows an example of a right atrial electrogram of induced atrial fibrillation and its surrogate time series. Phase space was reconstructed using embedding delays of 48 ms and 21 ms, respectively. The estimated correlation integrals of both of these time series are shown (middle panel) for embedding dimension 2 (top curve) to 20 (bottom curve) incremented by 2. The correlation integral at embedding dimension 10 is marked as a thick line. In the lower panel the original correlation integral is compared with the mean correlation integral of the ensemble of surrogate data at embedding dimension 10. It is observed that these curves differ significantly for normalized distances $r < 0.25$. Therefore we reject the null hypothesis that the local electrogram is generated by a linear stochastic system.

Results

Electrograms and phase plots

In Figure 7 unipolar electrograms are shown recorded from the right atrium during sinus rhythm, atrial flutter and three types of atrial fibrillation. The electrograms of sinus rhythm and atrial flutter showed a constant morphology and interval.

Electrograms of type I and II fibrillation mainly displayed discrete atrial activation complexes. A varying degree of ventricular response was observed. In particular, electrograms of patient 1 and 4 showed large ventricular deflections. Type III electrograms were charac-

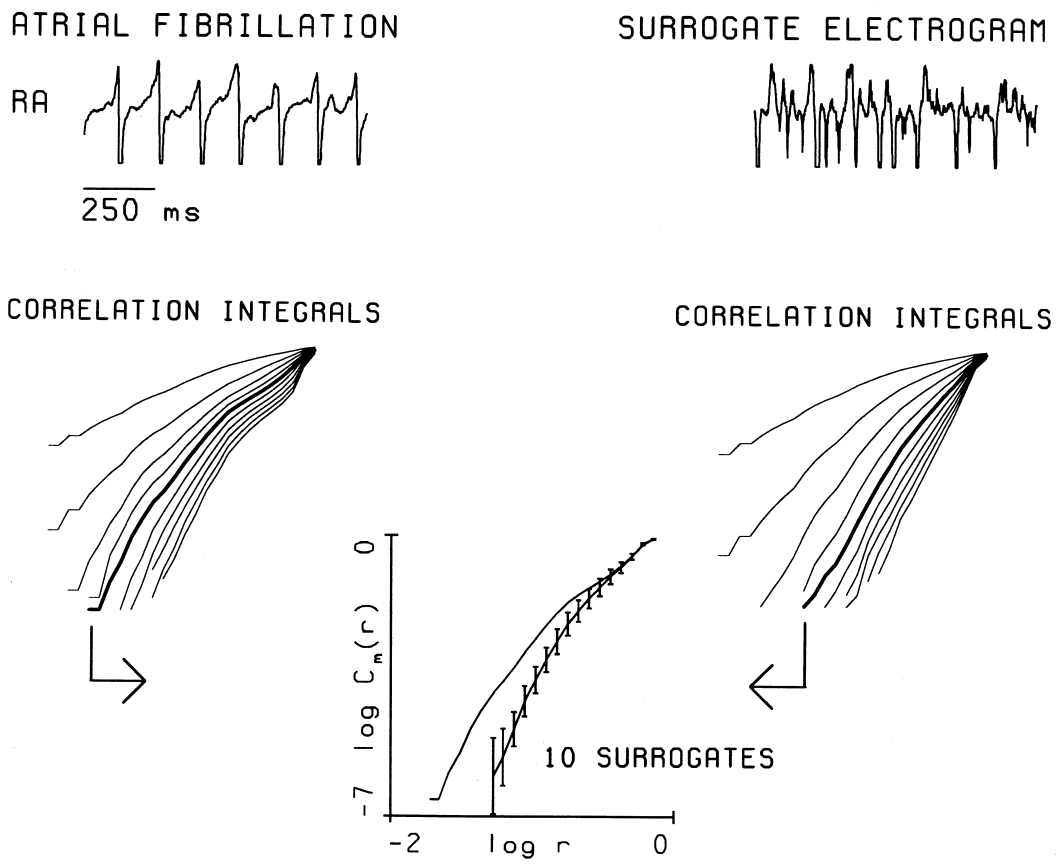

Figure 6: A right atrial unipolar electrogram (RA) of electrically induced atrial fibrillation (patient 2), and its phase randomized surrogate electrogram with the same linear dynamical properties and the original amplitude distribution. Double logarithmic plots show correlation integrals of the original electrogram and its surrogate time series for embedding dimensions 2 (top curve) to 20 (bottom curve), with an increment of 2. The embedding delay was 48 ms and 21 ms respectively. In the panel at the bottom the correlation integral $C_m(r)$ at embedding dimension $m = 10$ (thick line) of the original electrogram is plotted together with the averaged correlation integral of an ensemble of 10 surrogate electrograms. Error bars represent twice the standard deviation.

terized by fragmented complexes and multiple irregular deflections (Figure 7). Gain settings varied between patients and clipping of the signals occasionally occurred.

The discrete activation complexes resulting from uniform atrial activation generated a cross-like structure in phase plots of sinus rhythm (Figure 8). Additional fine structure was visible due to e.g. ventricular depolarisation and smaller local atrial deflections. In the phase plots of atrial flutter and atrial fibrillation, wave fronts also generated cross-like structures. In patient 1, trajectories followed a double cross due to large ventricular deflections. Irregular local atrial activation generated more complex phase plots (patient 6 to 9). A varying degree of fine structure was visible (e.g. in the phase plots of patient 5 and 6), because the signal amplification was set individually for different patients.

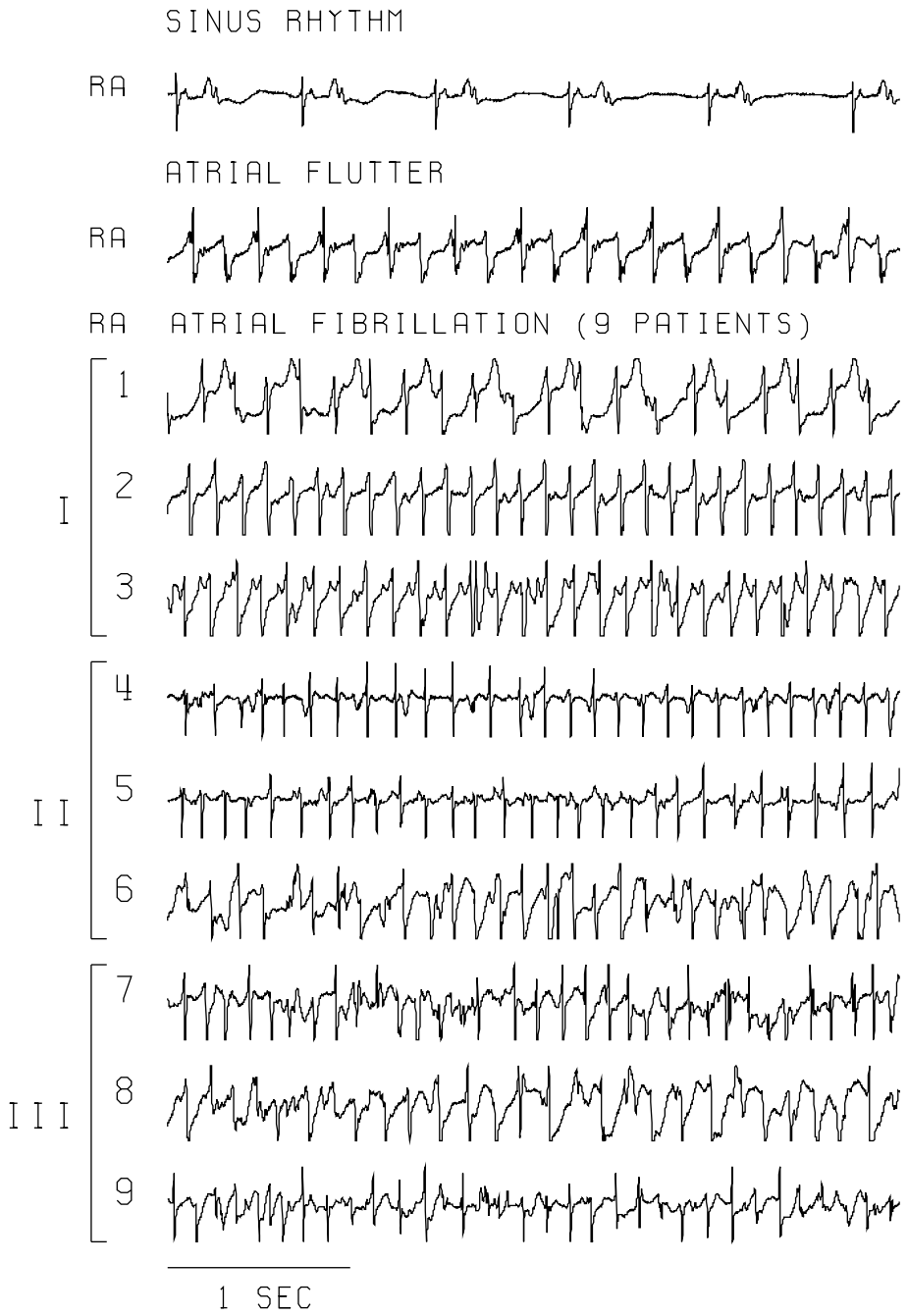

Figure 7: Right atrial unipolar epicardial electrograms (RA) during sinus rhythm, electrically induced atrial flutter and atrial fibrillation in 9 patients. The electrograms were measured at electrode position (c) as shown in Figure 1. Electrograms were amplified (gain typically 300 to 1000), filtered (bandwidth 1 to 500 Hz), AD converted (resolution 8 bits) and sampled at 1 kiloHerz. Electrograms of atrial fibrillation of type I (patients 1 to 3) mainly showed discrete atrial activation complexes. Electrograms of type II showed discrete activation complexes (patient 4 and 5) as well as irregular (patient 6) deflections. Electrograms of type III (patients 7 to 9) predominantly showed irregular deflections and fragmented activation complexes. Large ventricular deflections were present in the electrograms of patient 1 and 4.

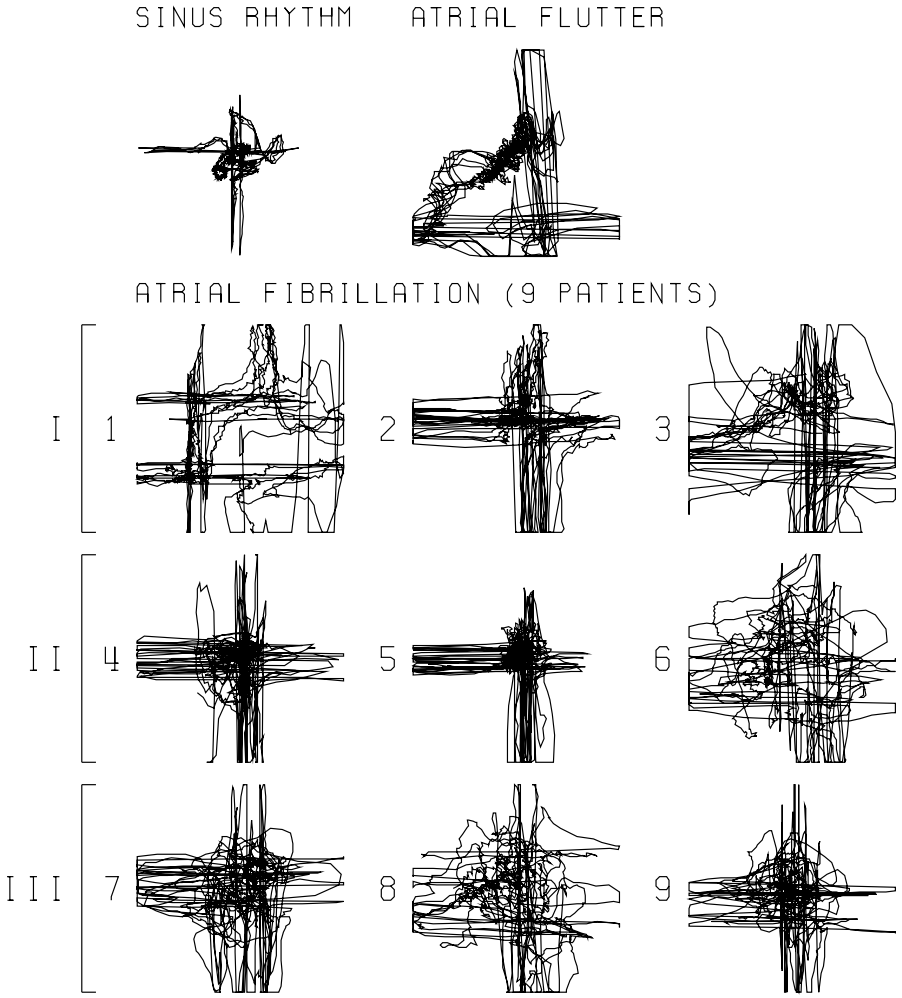

Figure 8: Phase plots of electrograms of sinus rhythm, electrically induced atrial flutter and atrial fibrillation of type I, II and III. Results are shown from electrograms measured at electrode position (c) as shown in Figure 1. Amplitude values along the abscissa are delayed with respect to values along the ordinate. See Figure 4 for scale calibration. The delays were 35 ms (sinus rhythm, patient 1), 14 ms (atrial flutter, patient 8), and 63, 51, 34, 18, 27, 38, 28, 40, 30 ms (atrial fibrillation, patient 1 to 9). Trajectories consist of the first 2000 points in the time series. Discrete atrial activation complexes generate a cross-like structure. In the case of sinus rhythm, additional fine structures are visible from e.g. ventricular deflections and smaller local atrial deflections. The phase plot of patient 1 during atrial fibrillation shows a double cross structure, caused by large ventricular deflections. Irregular local atrial activations generate complex structures in the phase plots of atrial fibrillation.

Correlation dimension and entropy

Figure 9 shows correlation integrals (left column), coarse-grained correlation dimension (middle column) and entropy (right column) for embedding dimension 2 to 20, incremented by 2. A scaling region (between dashed lines) was observed in correlation integrals of sinus rhythm and atrial flutter in the intervals [0.04-0.18] and [0.06-0.18] of normalized distance r, respectively. In plots of coarse-grained correlation dimension and entropy scaling was characterized by "plateauing", i.e. leveling-off of the curves with increasing embedding dimension.

Averaging correlation dimensions over embedding dimensions 15 to 19 resulted in $D = 3.8 \pm 0.1$ and $K = 2.0 \pm 0.1$ nats/s for the electrogram of sinus rhythm. The episode of atrial flutter was characterized by correlation dimension $D = 3.6 \pm 0.1$ and correlation entropy $K = 4.2 \pm 1.7$ nats/s, averaged over embedding dimensions 10 to 14.

During atrial fibrillation of type I, scaling was observed in correlation integrals of patient 2 and 3 at larger distances [0.21-0.42] and [0.25-0.50], respectively. Averaging over embedding dimensions 10 to 14 resulted in $D = 2.5 \pm 0.1$ and $K = 3.6 \pm 0.3$ nats/s (patient 2), and $D = 3.0 \pm 0.1$ and $K = 2.2 \pm 0.1$ nats/s (patient 3).

Electrograms were also characterized at embedding dimension 10 and at a coarse-grained distance r_{cg} corresponding to the normalized standard deviation of electrograms (asterisk). For sinus rhythm we obtained a coarse-grained dimension $D_{cg} = 3.1$, and coarse-grained entropy $K_{cg} = 6.9$ nats/s ($r_{cg} = 0.09$). Atrial flutter was characterized by $D_{cg} = 2.8$ and $K_{cg} = 6.8$ nats/s ($r_{cg} = 0.17$).

Going from type I to type III fibrillation the coarse-grained correlation dimension gradually increased from 2.4 to 9.3. Coarse-grained correlation entropy also increased from 3.3 to 27.3 nats/s. Coarse-grained resolution r_{cg} calculated for the electrograms of atrial fibrillation was typically in the range of 0.1 to 0.2 of normalized distance r.

Coarse-grained correlation dimension and entropy of type I fibrillation showed plateauing in patient 2 and 3. In type II fibrillation, curves of coarse-grained correlation dimension had a tendency to level-off at large distances, however no clear scaling plateaus were formed. Correlation integrals of type III fibrillation were steep, without any indication of scaling. In type II and III of atrial fibrillation, curves of coarse-grained correlation entropy showed rapidly increasing behaviour towards smaller distances.

Furthermore, we analyzed four additional simultaneously recorded electrograms at different electrode positions to investigate the effect of local variability in the mapping area. Table 3 summarizes the results of the nonlinear analysis applied to electrograms recorded at the positions (a) to (e) indicated in Figure 1. Figure 10 shows the ranking of the patients according to increasing coarse-grained correlation dimension D_{cg} and entropy K_{cg} averaged over the five electrode positions. Coarse-grained correlation dimension and entropy were relatively small when the atrium is activated by single broad wavefronts like e.g. in sinus rhythm or atrial flutter. The coarse-grained correlation dimension was 2.4 ± 1.5 (mean $\pm$ SD) and 2.7 ± 0.6, respectively. The coarse-grained correlation entropy was 5.1 ± 2.3

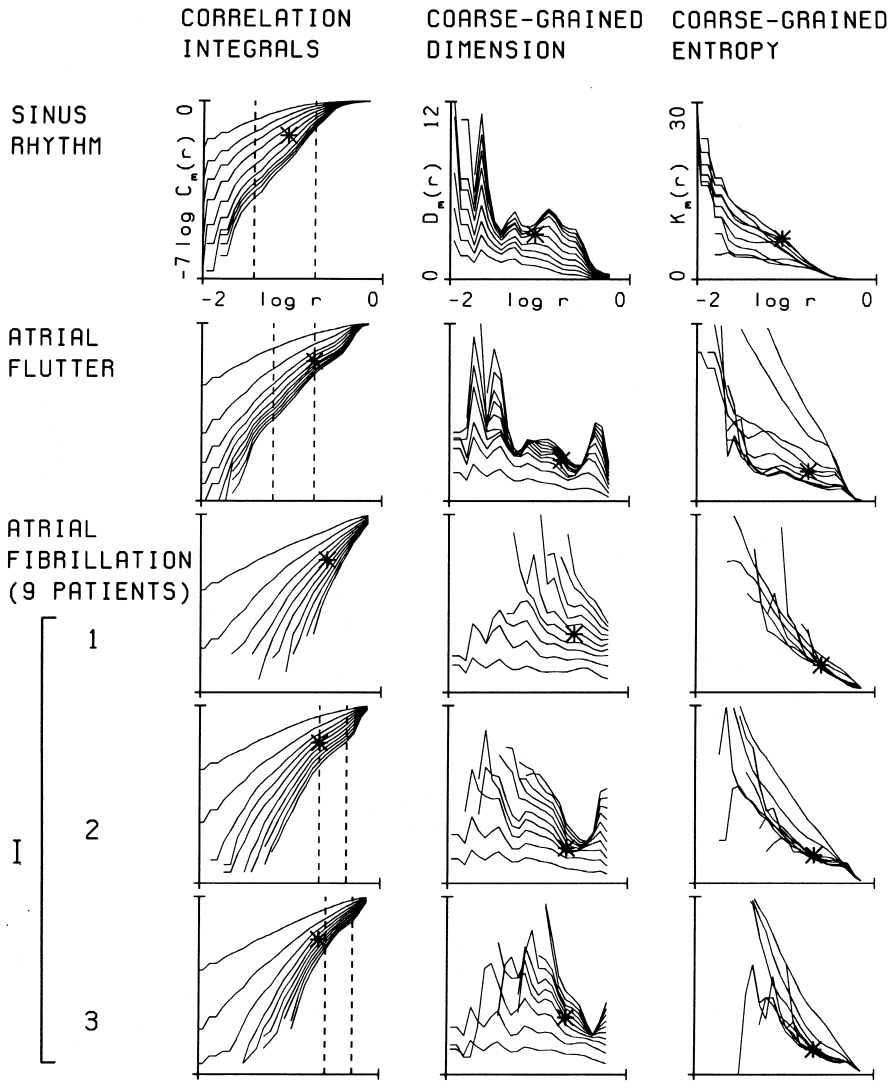

Figure 9: Correlation integrals $C_m(r)$ (left column), coarse-grained dimension $D_m(r)$ (middle column), and coarse-grained entropy $K_m(r)$ (right column) of sinus rhythm (16 seconds, patient 1), electrically induced atrial flutter (6 seconds, patient 8) and atrial fibrillation (4 seconds) of type I (patient 1 to 3), type II (patient 4 to 6) and type III (patient 7 to 9). Results are shown from electrograms measured at electrode position (c) as shown in Figure 1. Coarse-grained dimension and entropy were estimated at embedding dimension 10 and at a coarse-grained resolution (asterisk), corresponding to a normalized standard deviation of the electrograms. During episodes of sinus rhythm and atrial flutter scaling regions (between dashed lines) were [0.04-0.18] and [0.06-0.18], respectively. Scaling was reflected by "plateauing" of the coarse-grained dimension and entropy in the scaling region as a function of increasing embedding dimension. In electrograms of atrial fibrillation of type I a scaling region was identified in the intervals [0.21-0.42] (patient 2) and [0.25-0.50] (patient 3) of normalized distance r.

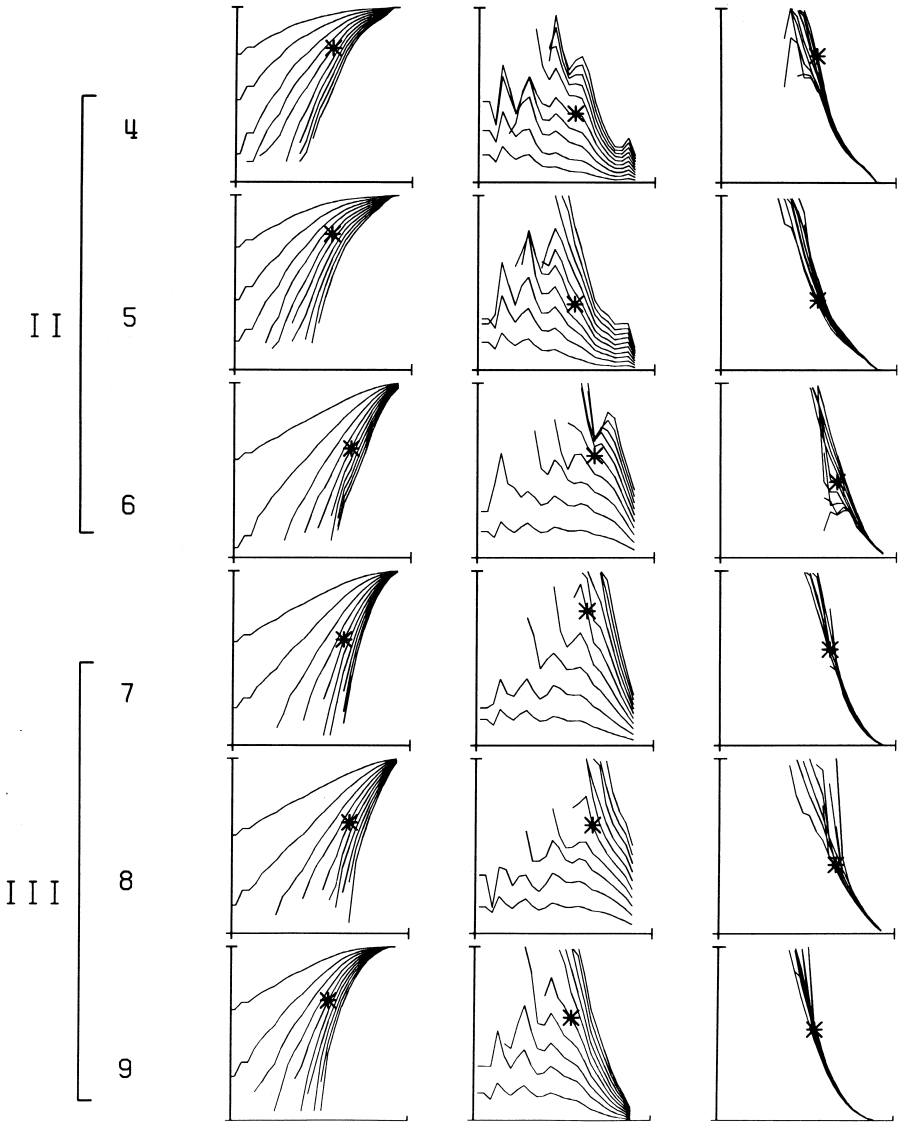

Figure 9, *continued.*

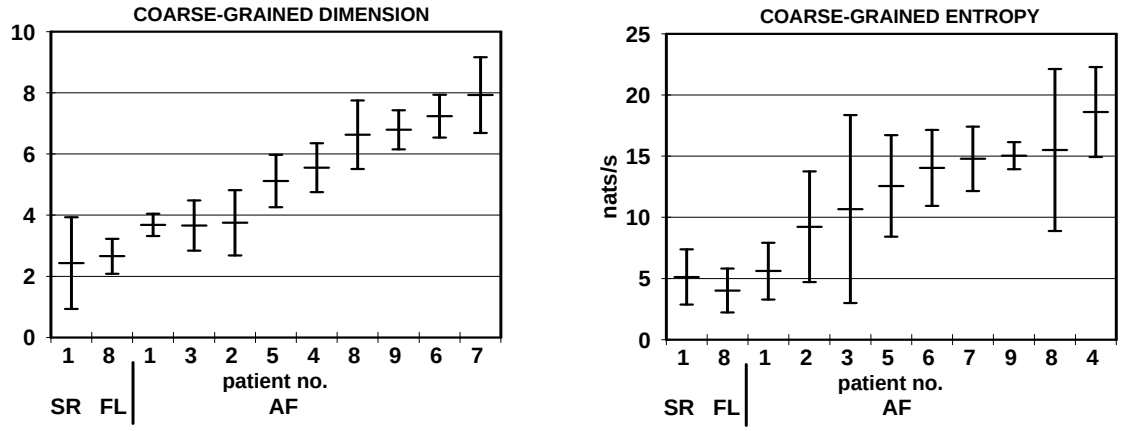

Figure 10: Coarse-grained dimension and coarse-grained entropy averaged over five electrograms during sinus rhythm (SR), electrically induced atrial flutter (FL) and atrial fibrillation (AF) of type I, II and III in nine patients. The patients are ranked according to increasing coarse-grained dimension and entropy estimated during AF. Results were obtained at embedding dimension 10 and at a coarse-grained resolution corresponding to a normalized standard deviation of the electrograms. Error bars correspond to the width of one standard deviation.

nats/s in sinus rhythm and 4.0 $\pm$ 1.8 nats/s in atrial flutter. Atrial fibrillation of type I was characterized by a mean coarse-grained correlation dimension between 3 and 4. As the activation patterns got more complex, its value increased up to values between 5 and 8 in type II and III fibrillation. The mean coarse-grained correlation entropy gradually increased in atrial fibrillation from values of about 5 nats/s in type I leveling off at about 15 nats/s in type III.

Comparison with surrogate electrograms

The original correlation integral at embedding dimension 10 was compared with the mean correlation integral generated by the ensemble of 10 surrogate electrograms (Figure 11). The correlation integral of sinus rhythm differed significantly from the calculated mean surrogate integral at distances $r < 0.11$. Differences were also significant for atrial flutter and atrial fibrillation of type I. However, the divergence of the original and the mean surrogate correlation integral started at larger distances in phase space, typically in the range from 0.15 to 0.4 of normalized r.

In type II and III fibrillation the correlation integral could hardly be distinguished from the mean surrogate correlation integral. Although statistically significant at some intermediate distances r, the differences were not substantial.

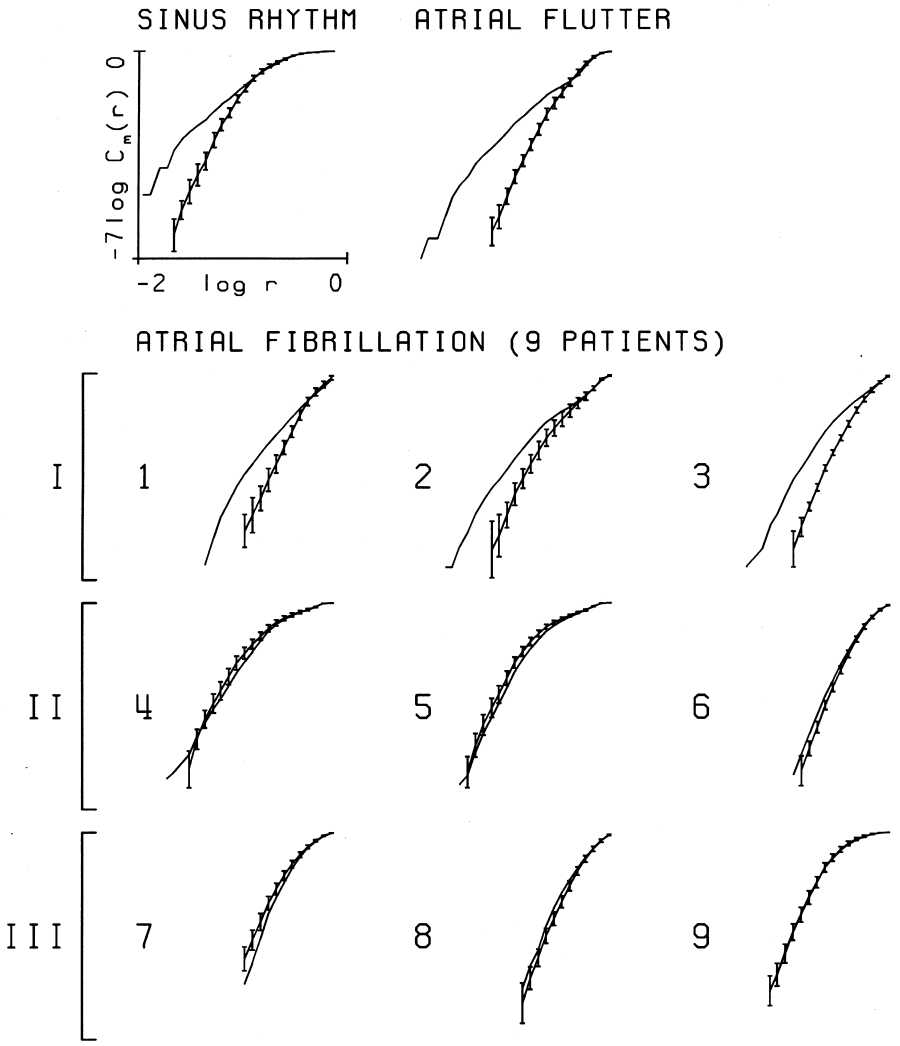

Figure 11: Correlation integral $C_m(r)$ at embedding dimension $m = 10$ of a right atrial electrogram and the averaged correlation integral of a set of 10 surrogate electrograms of sinus rhythm (patient 1), electrically induced atrial flutter (patient 8) and atrial fibrillation of type I (patient 1 to 3), type II (patient 4 to 6) and type III (patient 7 to 9). Results are shown from electrograms measured at electrode position (c) as shown in Figure 1. During sinus rhythm and atrial flutter, the original correlation integral at embedding dimension 10 (upper curve) differed significantly from the averaged correlation integral of the set of 10 surrogate electrograms (lower curve). During atrial fibrillation only a significant difference was found in fibrillation of type I (patients 1 to 3). In all other cases of atrial fibrillation the correlation integral did not differ significantly from the averaged correlation integral of the ensemble of surrogate electrograms. Error bars represent twice the standard deviation.

Table 3
Results of Nonlinear Analysis

rhythm	patient no.	D_{cg}	K_{cg} nats/s	scaling region (normalized r)	D	K nats/s	Nonlinearity
SR	1	2.6	2.5	0.04-0.13	3.3 ± 0.3*	3.3 ± 0.4*	+
		4.5	2.9	0.03-0.07	5.1 ± 0.5	4.7 ± 0.8	+
		3.1	6.9	0.04-0.18	3.8 ± 0.1	2.0 ± 0.1	+
		1.4	7.3	0.06-0.15	2.3 ± 0.2	7.6 ± 1.7	+
		0.7	5.9	0.06-0.15	1.0 ± 0.1	8.6 ± 1.1	+
		2.4 ± 1.5**	5.1 ± 2.3**				
FL	8	1.7	3.0	0.06-0.15	3.1 ± 0.2	3.4 ± 0.8	+
		3.0	2.9	0.06-0.18	4.2 ± 0.2	3.1 ± 0.3	+
		2.8	6.8	0.06-0.18	3.6 ± 0.1	4.2 ± 1.7	+
		2.7	2.6	0.09-0.21	2.7 ± 0.1	2.2 ± 0.1	+
		3.1	4.8	0.11-0.25	3.7 ± 0.2	3.8 ± 0.1	+
		2.7 ± 0.6	4.0 ± 1.8				
AF I	1	3.7	6.5	—	—	—	+
		3.2	4.6	—	—	—	+
		3.9	4.6	—	—	—	+
		4.1	3.3	—	—	—	+
		3.4	9.2	—	—	—	+
		3.7±0.4	5.6±2.3				
	2	4.9	14.9	—	—	—	+
		3.4	4.9	0.21-0.42	3.2 ± 0.2	3.5 ± 0.6	+
		2.4	4.7	0.21-0.42	2.5 ± 0.1	3.6 ± 0.3	+
		4.8	9.1	—	—	—	+
		3.4	12.5	—	—	—	+
		3.8±1.1	9.2±4.5				
	3	3.1	6.4	0.21-0.42	2.6 ± 0.1	3.8 ± 0.4	+
		4.4	17.2	—	—	—	—
		3.9	4.2	0.25-0.50	3.0 ± 0.1	2.2 ± 0.1	+
		2.5	4.9	0.25-0.50	1.8 ± 0.1	2.8 ± 0.6	+
		4.4	20.7	—	—	—	—
		3.7±0.8	10.7±7.7				

SR sinus rhythm; FL atrial flutter; AF I to III atrial fibrillation of type I to III. Results are given for electrode positions (a) to (e) as indicated in Figure 1. D_{cg} coarse-grained correlation dimension; K_{cg} coarse-grained correlation entropy; D correlation dimension; K correlation entropy. *Mean ± SD, averaged over 5 estimated values in the range of saturation. **Mean ± SD. Nonlinearity is indicated positive (+) when the null hypothesis of linear stochastic dynamics is rejected.

Table 3, continued

Results of Nonlinear Analysis

rhythm	patient no.	D_{cg}	K_{cg} nats/s	scaling region (normalized r)	D	K nats/s	Nonlinearity
AF II	4	6.6	22.2	—	—	—	—
		6.1	14.7	—	—	—	—
		4.7	21.8	—	—	—	—
		4.9	19.5	—	—	—	—
		5.5	14.8	—	—	—	—
		5.6±0.8**	18.6±3.7**				
	5	4.7	8.3	—	—	—	—
		4.2	10.1	—	—	—	—
		4.5	12.0	—	—	—	—
		6.0	19.2	—	—	—	—
		6.1	13.2	—	—	—	—
		5.1±0.9	12.6±4.2				
	6	6.1	11.5	—	—	—	—
		7.8	11.0	—	—	—	—
		7.0	13.0	—	—	—	—
		7.7	17.3	—	—	—	—
		7.5	17.4	—	—	—	—
		7.2±0.7	14.1±3.1				
AF III	7	8.2	17.6	—	—	—	—
		8.5	14.0	—	—	—	—
		9.3	16.5	—	—	—	+
		7.8	10.8	—	—	—	—
		5.9	15.1	—	—	—	—
		7.9±1.2	14.8±2.6				
	8	5.0	12.0	—	—	—	—
		5.9	13.4	—	—	—	—
		7.4	11.8	—	—	—	—
		7.3	13.0	—	—	—	—
		7.5	27.3	—	—	—	—
		6.6±1.1	15.5±6.6				
	9	6.8	13.8	—	—	—	—
		6.0	14.2	—	—	—	—
		7.1	15.8	—	—	—	—
		7.7	16.4	—	—	—	—
		6.4	15.0	—	—	—	—
		6.8±0.6	15.0±1.1				

Discussion

For reasons of mathematical simplicity time series are often analysed by methods only suited for linear systems, e.g. Fourier analysis. However, it is now recognized that these methods are of limited value since in general observed time series originate from intrinsic nonlinearities present in the underlying dynamics. Recently, a considerable interest has risen in the theory of nonlinear dynamical systems, which provides methods to extract quantities from a measured time series which are genuine characteristics of the dynamical behaviour of the system. This started with the rediscovery that simple nonlinear physical systems (e.g. a driven pendulum) can exhibit complicated dynamical behaviour. Also it is now well established that irregular behaviour of some very complicated systems (e.g. fluids near the onset of turbulence) can be understood with relatively simple models involving only a few degrees of freedom.

The quintessence of nonlinear time series analysis is the systematic quantitative comparison of all the segments obtained from a time series while varying their lengths. Essential ingredients used are concepts such as a dynamical system, phase space and reconstruction of the dynamics. The results of the nonlinear analysis are independent of the mode of description and limit the set of possible models suitable to describe the dynamics of the system. By comparing the obtained quantities such as correlation dimension and entropy one may in principle characterize different types of time series and classify dynamical systems. Our ultimate aim is to describe the electrical activity of the heart in space and time and to get insight into the underlying physiological processes from the measured electrograms.

It has become increasingly clear that the methods which have been developed to characterize nonlinear dynamical systems from experimental time series may easily produce spurious results if the algorithms are not applied with extreme care. Furthermore, physiological time series are often rather short, noisy and nonstationary, putting additional restrictions to the validity of the tools of nonlinear analysis. In the following we will discuss some of the limitations of this study with regards to both the methods used and the data available for the analysis.

Reconstruction of dynamics

The nonlinear analysis of experimental time series is based on Takens' reconstruction theorem. This theorem has been mathematically proven for stationary, infinitely long, noise free data sets and the reconstruction parameters, such as the sampling period and the embedding delay can be chosen almost arbitrarily.

In practice, however, time series are of finite length and contaminated with an unknown amount of noise. Furthermore, physiological time series are nearly always nonstationary and it is common practice to select the length of the time series with the naked eye. In this study, the electrograms were filtered with an upper cut-off frequency of 500 Hz. Although

this is sufficient for high-density mapping as performed by Konings et al.,[3] it should be remarked that at a more detailed level in some atrial tissues there are components of the extracellular waveforms that have a higher frequency content than 500 Hz (cf.[20]), so that we may not have used all the relevant information obtainable from unipolar electrograms in our nonlinear analysis.

Also, the embedding dimension m and the embedding delay τ are to be chosen optimally. At present the choice of these reconstruction parameters is a matter of empiricism. The dynamics are faithfully reconstructed by the delay vectors (eq. 1) when the embedding dimension m is sufficiently large. It is our experience that a maximal embedding dimension of 20 is appropriate. We decided to take the embedding delay equal to the first minimum of the mutual information function of the time series,[21] minimizing redundancy between consecutive lagged components of the delay vectors (eq. 1). Ever since the introduction of mutual information as an estimator for the embedding delay it has been a popular choice, although many alternative proposals have been made.[22] For the electrograms of atrial fibrillation this choice of the embedding delay corresponded to about one quarter of the characteristic period (typically about 30 to 40 ms).

It has been shown by Theiler[23] that delay vectors in phase space with time separations smaller than the autocorrelation time of the time series give spurious contributions to the correlation integral in short data sets, underestimating the correlation dimension. A procedure to avoid this is to exclude delay vectors which lie closer in time than the first minimum of the mutual information function. To be on the safe side we took twice this value.

Choice of coarse-grained parameters

To estimate the coarse-grained correlation dimension and entropy additional reconstruction parameters have to be chosen. It appears plausible to choose for the coarse-grained resolution in phase space a characteristic value of each individual electrogram. Furthermore we choose a common value for the embedding dimension in all electrograms. To avoid that the coarse-grained resolution lies in the region dominated by statistical scatter and noise, a compromise had to be made between the choice of an embedding dimension and a suitable coarse-grained resolution. We opted for an embedding dimension of 10 and a coarse-grained resolution equal to the standard deviation of the electrogram divided by the largest absolute difference of the amplitudes of the electrograms.

We do not claim that in both the reconstruction of the dynamics and the estimation of the coarse-grained correlation dimension and entropy the choice of the reconstruction parameters is optimal in any sense. However, the choices made led to a procedure to discriminate between the electrograms of different patients. It remains a challenging problem how to choose the reconstruction parameters optimally for time series such as local fibrillation electrograms.

Noise and clipping

A major obstacle in the nonlinear analysis of time series in general and of physiological time series in particular is the presence of measurement noise (e.g. electrode noise) and dynamical noise resulting from fluctuations generated in the organism itself. Also clipping of the signal can not always be avoided. To get some insight into their effects we applied a moving average filter to the electrograms. The filter transfer function is given by

$$y(t_i) = \frac{1}{2M+1}\left\{h(t_i) + \sum_{k=1}^{M} h(t_{i-k}) + h(t_{i+k})\right\}, \tag{2}$$

where $h(t_i)$ are the values taken from the original time series, and $y(t_i)$ is the filter output at a given discrete time t_i. The averaging window $2M$ was equal to 16 ms, corresponding to about the width of local activation complexes in electrograms of atrial fibrillation. The filtering smoothens the electrograms, so that noise and the effect of clipping were reduced.

The effects of the filtering on the calculations were checked for an example of atrial fibrillation of type I (patient 3). The average over five electrograms yielded $D_{cg} = 3.8 \pm 1.1$ and $K_{cg} = 9.2 \pm 6.9$ nats/s. Moving average filtering hardly affected the observed scaling regions and introduced only minor changes in the estimated correlation dimension and entropy (see table 3).

Effect of ventricular response

Unipolar electrograms contain contributions of extracellular potentials from all active current sources of the heart. These volume conduction effects cause far field pick-up of ventricular depolarization in local atrial electrograms. To study the electrical activity due to atrial fibrillation only, the ventricular response is a confounding factor. Unfortunately, the local atrial electrograms of 4 seconds duration are too short to remove the ventricular response accurately.

To get a first impression of their effects, we removed ventricular deflections by a coherent averaging procedure. First, a template QRS window was determined from a surface ECG, detecting the R-waves and averaging the QRS intervals. Next, the template QRS window was centered around each detected R-wave and the deflections within these windows were averaged in the atrial electrogram. Finally, the resulting averaged waveform was subtracted from the original electrogram within each QRS window centered around subsequent R-waves.

We analyzed the five electrograms of patient 4, which showed large ventricular deflections. After coherent averaging the coarse-grained correlation dimension D_{cg} decreased from 5.6 ± 0.8 to 4.5 ± 0.9, while the coarse-grained correlation entropy K_{cg} decreased from 18.6 ± 3.7 to 13.6 ± 5.7 nats/s. Furthermore, we applied coherent averaging to the five electrograms of patient 1, which also showed large ventricular deflections. D_{cg} increased from 3.7 ± 0.4 to 4.2 ± 0.6, while K_{cg} decreased from 5.6 ± 2.3 to 4.8 ± 1.1 nats/s. The five electrograms

Table 4
Classification of atrial fibrillation

Type	I			II			III		
maps	1	2	3	4	5	6	7	8	9
D_{cg}	3	2	1	4	5	8	9	6	7
K_{cg}	1	2	3	5	4	6	7	9	8

Ranking of patients (from left to right) according to increasing spatio-temporal complexity (maps), coarse-grained correlation dimension (D_{cg}) and coarse-grained correlation entropy (K_{cg}). Numbering refers to patient numbers. Type I, II, III indicate the three types of atrial fibrillation in the study of Konings et al.[3] QRS complex has been removed by coherent averaging in electrograms of patient 1 and 4.

of patient 9 did not show large ventricular responses. After coherent averaging D_{cg} changed from 6.8 ± 0.6 to 6.9 ± 0.6 while K_{cg} changed from 15.0 ± 1.1 to 16.5 ± 1.3 nats/s.

We thus see that the incidence of ventricular deflections during atrial fibrillation may cause an appreciable change in the coarse-grained dimension and coarse-grained entropy compared to the electrogram in which ventricular deflections were removed.

Relation of nonlinear analysis of atrial fibrillation to high-density mapping

In the high-density mapping study of Konings et al.[3] the patients were classified according to the degree of complexity of right atrial activation patterns during atrial fibrillation. Three types of atrial fibrillation (I, II, III) were defined based on the observed continuous spectrum of increasing spatio-temporal complexity.

We ranked the patients according to increasing coarse-grained correlation dimension D_{cg} and entropy K_{cg} (Figure 10). It was observed that patient 4, which is classified by mapping as type II, had maximal coarse-grained entropy in the group of nine patients. Large ventricular deflections were present in the electrograms of this patient, due to the incidence of QRS complexes. After removing the QRS complexes by coherent averaging, both K_{cg} and D_{cg} considerably decreased (27 and 20 % respectively). Also the large ventricular deflections due to the incidence of QRS complexes in the electrograms of patient 1 were removed, resulting in a somewhat increased D_{cg} (14 %) and decreased K_{cg} (14 %).

In Table 4, the patients are ranked according to increasing spatio-temporal complexity (maps), coarse-grained correlation dimension (D_{cg}) and coarse-grained correlation entropy (K_{cg}). Note that QRS complexes have been removed in patient 1 and 4 by coherent averaging. We find for the coarse-grained correlation entropy a classification of the nine patients into three groups corresponding with the three types characterized from the high-density maps. This is also true for the ranking of patients by the coarse-grained correlation dimension with

one exception (patient 6). However, this exception lies on the border of type II and III. It should be emphasized that only 5 local electrograms of 4 seconds duration were used in the nonlinear analysis, whereas the classification of activation patterns is based on the analysis of 244 electrodes in a 12 second time window.

Thus, the classification using nonlinear analysis correlates fairly well with the characterization of activation patterns determined from high-density mapping. We conclude that the classification of electrically induced atrial fibrilation resulting from the nonlinear analysis of five local right atrial electrograms is consistent with the proposed classification of human right atrial activation as visualized from high-density mapping.[3]

Dynamical characteristics of electrograms

Sinus rhythm and atrial flutter

It has been suggested[6] that normal sinus rhythm is generated by chaotic dynamics. Estimates of the correlation dimension of sinus rhythm have been reported[6] ranging from 3.6 to 5.2 in four different healthy subjects using ECG recordings of 4 minutes (60000 points). Using time series of only a few thousand RR intervals the correlation dimension was estimated to be about 6. Furthermore, for the correlation entropy about 1 nats/s was found. On the other hand, in a study in ten healthy subjects[8] series of about 4000 RR intervals were used and a correlation dimension of about 8.5 was reported. Nonlinear prediction and the method of surrogate data provided weak evidence for nonlinearity in the dynamics[7,8] so that it cannot be concluded from these observations that the dynamics of sinus rhythm is generated by low-dimensional chaos.

We analyzed five local electrograms of an episode of sinus rhythm in one patient and five local electrograms of an episode of electrically induced atrial flutter in another. The method of surrogate data indicates that there is a nonlinearity present in both sinus rhythm and electrically induced atrial flutter. Although the estimated correlation dimension and correlation entropy (Table 3) indicate that all electrograms analyzed show features of low-dimensional chaos in these particular episodes of sinus rhythm and atrial flutter, many more electrograms of varying duration in several subjects have to be analyzed before firm conclusions about their dynamics can be drawn.

Electrically induced atrial fibrillation

The method of surrogate data indicates the presence of a nonlinearity in nearly all electrograms of atrial fibrillation of type I. Electrograms of atrial fibrillation of type II and III could not be distinguished from time series generated by linear stochastic dynamics. Furthermore, the coarse-grained correlation dimension and entropy both show an increase in going from type I to III fibrillation. These results indicate that fully developed atrial fibrillation (type III) does not show features of low-dimensional chaos. This is consistent with

earlier studies applying methods from nonlinear dynamics to short surface ECG recordings from four dogs in ventricular fibrillation,[24] which suggest that the underlying mechanism is of high-dimensional nature.

In principle, for spatially extended systems like the heart, measurements at one fixed point on the atria should contain sufficient information to reconstruct and characterize the dynamics provided the system is finite and the various parts are sufficiently coupled.[25] When we have access to time series simultaneously measured at many points in space (spatio-temporal time series), it is interesting to use several electrograms measured at different points to reconstruct the dynamics. This can be done by a natural generalization of Takens' reconstruction methodology.[26,27] Currently, research is carried out to estimate correlation dimension and entropy from multiple electrograms using spatio-temporal reconstruction of the dynamics. The multivariate nonlinear analysis accounts for the many spatial degrees of freedom involved and offers the possibility to study spatio-temporal chaos in the observed time series of atrial fibrillation. The results obtained for the five electrograms in each patient suggest that the dynamics are quite "homogeneous" over the atrium and that spatio-temporal reconstruction of the dynamics may give additional information about the organisation of electrical activity during fibrillation.

Recently, the correlation length during electrically induced ventricular fibrillation has been estimated in five pigs to be approximately 4 to 10 mm.[28] Although this is much smaller than the scale of the heart, it does indicate some coherency. It has been suggested that atrial fibrillation in humans is not entirely random, and that activation fronts follow paths of previous excitation.[29] Also mapping studies[1] have demonstrated that a critical number of wavelets is needed for the perpetuation of atrial fibrillation, which might indicate an underlying spatial organization. It is therefore interesting to quantify the degree of spatial coherency in atrial fibrillation by estimating the correlation length in activation patterns of electrically induced atrial fibrillation using e.g. extensions to information-theoretic quantities.[30]

In summary, we have shown in this study that mathematical methods from the theory of nonlinear dynamics can be used to discriminate between different types of atrial fibrillation in humans.

Acknowledgement. We wish to thank Karen Konings for her assistance with the data selection and the high-density maps.

Appendix

In this section we present the details of the estimation of the correlation integral using the Grassberger-Procaccia (GP) method. Furthermore we describe the implementation to estimate the (coarse-grained) correlation dimension and correlation entropy from the correlation integral.

The correlation integral

The correlation integral of a (chaotic) deterministic system has been shown to be given by[31]

$$C_m(r) = Ar^D e^{-m\tau K}, \tag{3}$$

where D is the correlation dimension, K the correlation entropy, A a constant, m the embedding dimension and τ the embedding delay. Equation 3 is valid in the limit of sufficiently small distance r in phase space and sufficiently large embedding dimension m.

Estimating the correlation integral

The correlation integral is estimated as

$$C_m(N,r) = \frac{1}{N_{\rm ref}N} \sum_{i\in\{i_{\rm ref}\}} \sum_{j\in\{|j-i|\geq W\}} \Theta(r - \|\vec{x}(t_i) - \vec{x}(t_j)\|), \tag{4}$$

where the Heaviside function Θ is 1 for positive arguments and 0 otherwise. The inner sum averages the number of points $\vec{x}(t_j)$ (delay vectors, eq. 1) found within a hypersphere of radius r centered at point $\vec{x}(t_i)$ in reconstructed phase space of embedding dimension m. The outer sum averages the results over a set of $N_{\rm ref}$ reference points indexed $i_{\rm ref}$, which were randomly chosen from a total of N delay vectors. The embedding delay to construct the delay vectors was chosen equal to the first minimum of the mutual information function.[21] We choose $N_{\rm ref} = 1300$, corresponding to about one third of the length of the time series as suggested by Theiler.[32] In (eq. 4) we use the supremum norm

$$\|\vec{x}(t_i) - \vec{x}(t_j)\| = \max_{0\leq k<m} \mid x(i+k) - x(j+k) \mid \tag{5}$$

for computing efficiency. Before calculating the correlation integral, the time series is rescaled such that the difference between the minimal and maximal value of the time series becomes one. In this way the computed distances r are normalized by division through the largest absolute difference of the amplitudes of the signal. The correlation integral is computed up to 71 % of the maximum normalized distance $r_{\rm max} = 1$ for embedding dimensions m up to 20 at discrete distances r, using 4 divisions per binade.

Because electrograms are densely sampled, the correlation integral will contain distances from points which are close in time. To avoid spurious contributions to the correlation integral resulting from linear correlation between successive points in phase space,[23] a correction parameter W is included in (eq. 4), preventing the counting of distances resulting from vector pairs $(\vec{x}(t_i), \vec{x}(t_j))$ when $\mid i - j \mid < W$. In the calculation of correlation integrals we set W equal to twice the value of the first minimum of the mutual information function.

Using an optimized algorithm to find neighbouring points in reconstructed state space,[33] this implementation of the GP method typically takes about 1 minute of CPU time on an AXP 3000 DEC computer to calculate the set of 20 correlation integrals from a time series containing 4000 samples.

Estimating correlation dimension and entropy

The correlation integral is plotted on a double logarithmic scale (base 10) as a function of distance r. At a given embedding dimension m one then looks for a linear part, a so-called "scaling region", in this double logarithmic plot.

The correlation dimension D at embedding dimension m is estimated from the slope in the scaling region by linear regression through points $(\ln r, \ln C_m(r))$. In case D saturates as a function of m, this value is taken as the correlation dimension. D was estimated by averaging over five correlation dimensions in the range of convergence.

It is convenient to calculate the correlation entropy K at embedding dimension m using a nonlinear Levenberg-Marquardt fitting procedure applied simultaneously to two correlation integrals for r within the scaling region at embedding dimensions m and $m+1$. The correlation entropy is given using the natural logarithm in units nats/s, and is estimated by averaging over five correlation entropies in the range of convergence.

Estimating coarse-grained correlation dimension and entropy

Coarse-grained correlation dimension is defined by the local slope of the correlation integral,

$$D_m(r) = \frac{d \ln C_m(r)}{d \ln(r)}, \tag{6}$$

which is calculated numerically through three consecutive points $(\ln(r), \ln C_m(r))$. The distance r in eq. 6 corresponds to the distance of the central point of this triple.

Coarse-grained correlation entropy is defined by the logarithm of the quotient of two correlation integrals at embedding dimensions m and $m+n$, viz,

$$K_m(r) = \frac{1}{n\tau} \ln(\frac{C_m(r)}{C_{m+n}(r)}), \tag{7}$$

where τ is the embedding delay. We set $n = 2$ in eq. 7 to reduce fluctuations in the estimated $K_m(r)$.

We evaluated the coarse-grained correlation dimension (D_{cg}) and coarse-grained correlation entropy (K_{cg}) at embedding dimension $m = 10$. The coarse-grained resolution r_{cg} was chosen equal to a normalized standard deviation, which was calculated dividing the standard deviation of the electrogram by the largest absolute difference of the amplitudes of the signal.

Acknowledgment

We wish to thank Karen Konings for her assistance with the data selection and the high–density maps.

References

[1] Allessie MA, Lammers WJEP, Bonke FIM, et al: Experimental evaluation of Moe's multiple wavelet hypothesis of atrial fibrillation. In Zipes DP, Jalife J, eds: Cardiac electrophysiology and arrhythmias. Grune and Stratton Inc., New York, 1985, p.265.

[2] Wells JL, Karp RB, Kouchoukos NT, et al: Characterization of atrial fibrillation in man: studies following open heart surgery. Pacing Clin Electrophysiol 1978;1:426-438.

[3] Konings KTS, Kirchhof CJHJ, Smeets JRLM, et al: High-density mapping of electrically induced atrial fibrillation in humans. Circulation 1994;89:1665-1680.

[4] Takens F: Detecting strange attractors in turbulence. In Rand DA, Young L-S eds: Dynamical systems and turbulence. Lecture notes in mathematics, Vol. 898. Springer-Verlag, Berlin, 1981, p.366.

[5] Ott E, Sauer T, Yorke JA: Coping with chaos. Analysis of chaotic data and the exploitation of chaotic systems. Wiley and Sons, Inc., New York, 1994.

[6] Babloyantz A, Destexhe A: Is the normal heart a periodic oscillator? Biol Cybern 1988;58:203-211.

[7] Lefebre JH, Goodings DA: Predictability of normal heart rhythms and deterministic chaos. Chaos 1993;3:267-276.

[8] Kanters JK, Holstein-Rathlou N-H, Agner E: Lack of evidence for low-dimensional chaos in heart rate variability. J Cardiovasc Electrophysiol 1994;5:591-601.

[9] Skinner JE, Pratt CM, Vybiral T: A reduction in the correlation dimension of heartbeat intervals precedes imminent ventricular fibrillation in human subjects. Am Heart J 1993;125:731-743.

[10] Allessie MA, Hoeks APG, Schmitz GML, et al: On-line mapping system for the visualization of the electrical activation of the heart. Int J Card Imaging 1986;140:59-63.

[11] Ott E: Chaos in dynamical systems. Cambridge University Press, Cambridge, 1993.

[12] Wolf A, Swift JB, Swinney HL, et al: Determining Lyapunov exponents from a time series. Physica D 1985;16:285-317.

[13] Grassberger P, Procaccia I: Measuring the strangeness of strange attractors. Physica D 1983;9:189-207.

[14] Takens F: Invariants related to dimension and entropy. In Atas do 13° coloquio Brasileiro de matematica, Instituto de matematica pura e aplicada (IMPA), Rio de Janeiro, Brazil, 1983.

[15] Tsimring LS: Nested strange attractors in spatiotemporal chaotic systems. Phys Rev E 1993;48:3421-3426.

[16] Pincus SM: A regularity statistic for medical data analysis. J Clin Monit 1991;7:335-345.

[17] Gaspard P, Wang X-J: Noise, chaos and (ε, τ)-entropy per unit time. Phys Reports 1993;235:291-343.

[18] Theiler J, Eubank S, Longtin A, et al: Testing for nonlinearities in time series: the method of surrogate data. Physica D 1992;58:77-94.

[19] Theiler J, Galdrikian B, Longtin A, et al: Using surrogate data to detect nonlinearity in time series. In Casdagli M, ed: Nonlinear modeling and forecasting. Addison-Wesley Publishing Company, Inc., Reading, 1992, p.163.

[20] Cabo C, Wharton JM, Wolf PD, et al: Activation in unipolar cardiac electrograms: a frequency analysis. IEEE Trans Biomed Eng 1990;37:500-508.

[21] Fraser AM, Swinney HL: Independent coordinates for strange attractors from mutual information. Phys Rev A 1986;33:1134-1140.

[22] Rapp PE: A guide to dynamical analysis. Integr Physiol Behav Sci 1994;29:311-327.

[23] Theiler J: Spurious dimension from correlation algorithms applied to limited time-series data. Phys Rev A 1986;34:2427-2432.

[24] Kaplan DT, Cohen RJ: Is fibrillation chaos? Circ Res 1990;67:886-892.

[25] Grassberger P, Schreiber T, Shaffrath C: Nonlinear time sequence analysis. Int J Bifurc Chaos 1991;1:521-547.

[26] Eckmann J-P, Ruelle D: Ergodic theory of chaos and strange attractors. Rev Mod Phys 1985;57:617-656.

[27] Abarbanel HDI, Brown R, Sidorowich JJ, et al: The analysis of observed chaotic data in physical systems. Rev Mod Phys 1993;65:1331-1392.

[28] Bayly PV, Johnson EE, Wolf PD, et al: A quantitative measurement of spatial order in ventricular fibrillation. J Cardiovasc Electrophysiol 1993;4:533-546.

[29] Gerstenfeld ED, Sahakian AV, Swiryn S: Evidence for transient linking of atrial excitation during atrial fibrillation in humans. Circulation 1992;86:375-382.

[30] Prichard D, Theiler J: Generalized redundancies for time series analyis. Preprint, 1994.

[31] Grassberger P, Procaccia I: Estimation of the Kolmogorov entropy from a chaotic signal. Phys Rev A 1983;28:2591-2593.

[32] Theiler J: Statistical precision of dimension estimates. Phys Rev A 1990;41:3038-3051.

[33] Grassberger P: An optimized box-assisted algorithm for fractal dimensions. Phys Lett A 1990;148;63-68.